Available online at www.sciencedirect.com

ScienceDirect

journal homepage: www.elsevier.com/locate/he

Sintering behavior of $BaCe_{0.7}Zr_{0.1}Y_{0.2}O_{3-\delta}$ electrolyte at 1150 °C with the utilization of CuO and Bi_2O_3 as sintering aids and its electrical performance

Zaheer Ud Din Babar [a,1], *Muhammad Bilal Hanif* [a,b,1], *Jiu-Tao Gao* [a], *Chang-Jiu Li* [a], *Cheng-Xin Li* [a,*]

[a] *State Key Laboratory for Mechanical Behavior of Materials, School of Materials Science and Engineering, Xi'an Jiaotong University, Xi'an, Shaanxi, China*

[b] *Department of Inorganic Chemistry, Faculty of Natural Sciences, Comenius University in Bratislava, Bratislava 84215, Slovakia*

HIGHLIGHTS

- BCZY sintered at low operating temperature of 1150 °C by using CuO and Bi_2O_3 as a sintering aid.
- 2 mol% CuO-Bi_2O_3 sintering aids are proven effective in getting denser structure.
- BCZY-2 shows high ionic conductivity of 0.85×10^{-2} at a low temperature of 600 °C.
- BCZY-2 shows activation energy of 0.41 eV which is a potential electrolyte for SOFCs application.

GRAPHICAL ABSTRACT

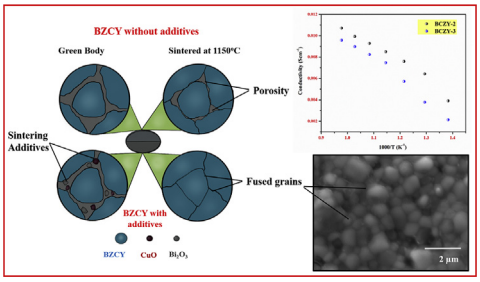

ARTICLE INFO

Article history:
Received 18 July 2021
Received in revised form
30 September 2021
Accepted 7 December 2021
Available online 29 December 2021

Keywords:
$BaCe_{0.7}Zr_{0.1}Y_{0.2}O_{3-\delta}$
Sinterability
Densification

ABSTRACT

$BaCe_{0.7}Zr_{0.1}Y_{0.2}O_{3-\delta}$ (BCZY) is one of the promising electrolytic candidate for solid oxide fuel cell (SOFC) due to its good proton conductivity and better stability. Herein, the effect of dual sintering aids such as CuO-Bi_2O_3 upon the sinterability at low temperature, improved electrochemical properties, and thermo-chemical changes about proton-conducting $BaCe_{0.7}Zr_{0.1}Y_{0.2}O_{3-\delta}$ electrolyte were investigated in detail. FESEM micrographs and shrinkage curves revealed significant improvement in sinterability and densifications of BCZY electrolyte. The dense pellets were sintered with CuO-Bi_2O_3 (2–3 mol %) as sintering aids at a temperature of 1150 °C for 5 h. The perfectly uniform distribution of sintering aids increased the linear shrinkage of BCZY from 5% till 19–21%. The crystallite size and grain growth within the structure was enhanced due to the formation of the melting phase of Bi_2O_3 and Cu^{2+} incorporation in the perovskite structure. The elevated and improved

* *Corresponding author.*
E-mail address: licx@mail.xjtu.edu.cn (C.-X. Li).
[1] Equal contribution.

https://doi.org/10.1016/j.ijhydene.2021.12.075

$CuO\text{-}Bi_2O_3$
Solid oxide fuel cell

electrochemical measurement for BCZY with 2 mol% of $CuO\text{-}Bi_2O_3$ as sintering aid categorized it well suited for solid oxide fuel cells.

Introduction

The rising threat to environment due to fossil fuel emission pushes the world to divert its attention towards renewable energy. Fuel cells have the potential to cope with the present energy demand of the globe because of their efficiency, stability, and wide range of applications, especially in the transport sector. At present proton-conducting electrolytes have emerged as an effective candidate in the enhancement of SOFCs technologies at intermediate temperatures [1–6].

Perovskites have been attracting much attention due to their various potential applications as solid electrolytes in SOFCs. Among various kinds of perovskite materials, doped BCZY has been investigated extensively and is reported with good stability and relatively high protonic conductivity [7–10]. However, the required densification of BCZY is possible to be obtained only at a higher sintering temperature usually greater than 1500 °C. And the elevated sintering temperature leads barium towards evaporation and subsequently segregation of doped elements is occurred. Furthermore, the porous structure of electrodes is difficult to be maintained at higher temperatures and due to the formation of impure phases, the electrochemical properties of BCZY electrolytes are significantly reduced [10,11].

The utilization of sintering aids is indicated as an effective way to reduce the sintering temperature and improve the electrochemical properties of ceramic materials. In ABO_3 type perovskite, such as BCZY, the proton conduction/migration is made via Grotthuss mechanism through a fixed vacant oxygen site known as vacancies [12–14]. Structural and chemical parameters determine oxygen defects hence, the proton conduction and can be altered with varying doped elements. Previously, various sintering aids such as ZnO, Li_2O, NiO, CuO, MgO, CoO, and Bi_2O_3, have been used to reduce the sintering temperature of different ceramic materials [15–22]. Similarly, the sintering behavior of BZCY is enhanced through the utilization of commonly used sintering aids i.e. NiO and ZnO either by internal doping and external addition [23–25]. In this way, $BaZr_{0.1}Ce_{0.66}Ni_{0.04}Y_{0.2}O_{3-\delta}$ electrolyte was prepared through an internal doping strategy with the reduction of sintering temperature from (1600–1400) °C whereas, the electrical conductivity was prominently enhanced. In addition, a perfectly dense electrolytic sheet is obtained by adding 0.5–1.0 wt% NiO externally at a reduced sintering temperature of 1400 °C. Liu et al. [26] reported the linear shrinkage rate of $Ba(Zr_{0.1}Ce_{0.7}Y_{0.2})O_{3-\delta}$ (BZCY7) as 14.25% (4.81% greater than the sample without NiO) with the addition of 0.5 wt% NiO. Bi et al. [27] synthesized $BaZr_{0.1}Ce_{0.66}Ni_{0.04}Y_{0.2}O_{3-\delta}$ solid solution from BCZY doped with NiO with improved electrolytic performance. Despite all the benefits, the addition of sintering aids may reduce the overall conductivity and open-circuit voltage due to impurity phases, because NiO is not completely dissolved into perovskite lattice and it reacts with BZCY resulting in the formation of BaY_2NiO_5 [28].

Tao et al. [29] reported the relative density of $BaCe_{0.5}Zr_{0.3}Y_{0.16}Zn_{0.04}O_{3-\delta}$ (i.e. BZCY added with ZnO) as 97%, at a reduced sintering temperature of 1325 °C. Wang et al. [30] added 4 mol % of ZnO to $BaCe_{0.5}Zr_{0.3}Y_{0.2}O_{2.9}$ and obtained higher conductivity with improved relative density. Several studies have reported the reduction of sintering temperature from 1300 to 1200 °C by the addition of ZnO but at the cost of decreased conductivity [31]. Zhao et al. [32] received a significant improvement in stability, relative density, and conductivity for BCZY added with ZnO at reduced sintering temperature but the grain boundary conductivity was hardly improved. At a sintering temperature of 1400 °C, the $BaZr_{0.1}Ce_{0.66}Ni_{0.04}Y_{0.2}O_{3-\delta}$ sample showed higher density with larger average grain size. Electrochemical test results for a sample doped with NiO revealed improved grain and grain boundary conductivity. Yining Li et al. used CuO up to 8% and reduce the sintering temperature of YSZ based cells from 1400 °C to 1100 °C, along with its mechanical strength which shows acceptable power output [50]. Whereas Tao Yang et al. proposed a new concept of lowering the sinterability of $BaZr_{0.85}Y_{0.15}O_{3-\delta}$ below 1400 °C by using NiO and ZnO as a sintering aid with densification above 95% [51].

O′ Hayre et al. [33] has investigated the influence of various sintering aids such as ZnO, CuO, Cr_2O_3, Fe_2O_3, Mn_2O_3, and PdO on the conductivity of BCZY electrolyte. The overall conductivity of the material was reduced due to the addition of ZnO, Cr_2O_3, Fe_2O_3, and Mn_2O_3 however, CuO and PdO were found effective to increase the electrical conductivity, with the only disadvantage of adding PdO was the reduced relative density of the sample. Similarly, the conducting properties of a sample were deteriorated due to the accumulation of excess ZnO at grain boundaries, being used as a sintering aid [23]. Therefore, it is still a challenging and attention-seeking task to effectively improve the densification of proton-conducting electrolytes while maintaining their conductivity.

In the recent studies, Bi_2O_3/CoO is used to reduce the sintering temperature of $Nd_{0.2}Ce_{0.8}O_{3-\delta}$ (NDC) electrolyte from 1400 °C to 1100 °C with improved densification and electrical properties [34]. CuO/Bi_2O_3 in 3 wt% was successfully utilized as a dual sintering aid in addition to $BaFe_{12}O_{19}$ at a temperature of 920 °C with improved magnetic properties [35]. $BaZr_{0.9}Y_{0.1}O_{3-\delta}$ (BZY) sintering temperature was reduced up to 1260 °C and electrical conductivity was enhanced by using ZnO/Na_3PO_4 [36]. The addition of NiO-Fe_2O_3 with 2 mol % $Ni_{0.5}Fe_{0.5}$ into BCZY was sintered at 1400 °C [37]. The sintering temperature of BCZY was reduced up to 1320 °C by using ZnO/Na_2CO_3 with linear shrinkage of

17.5% [38]. The combination of Li_2O/ZnO improved the sinterability of BZY as compared to individual utilization of either Li_2O or ZnO at a temperature of 1400 °C with the conductivity of 6.90 × 10^{-3} Scm^{-1} at 700 °C [39]. Previous literature has reported that low-melting Bi_2O_3 has significantly improved the material density due to the introduction of the liquid phase sintering effect [40–42]. CuO dopants are reported to contribute effectively towards the increased conductivity of materials as compared to other sintering aids. In general, the sintering additives can produce a larger grain size and specifically the substitutional doping of metal ions from perovskite structure is to increase the bulk proton concentration. However, the sintering behavior of BCZY electrolyte with the combined effect of CuO and Bi_2O_3 dopant has not been investigated yet.

In the current study, CuO and Bi_2O_3 were used as dual sintering aids to reduce the sintering temperature of BCZY electrolytes. The effect of sintering additives on densification and sintering behavior of BCZY electrolyte at low temperature i.e., 1150 °C was extensively investigated by utilizing the additives in various amounts/proportions. The electrochemical performance and thermo-chemical variations due to sintering additives were also explored via EIS and TGA/DSC analysis.

Experimental section

Powder synthesis

The freeze-drying method was followed for the preparation of $BaCe_{0.7}Zr_{0.1}Y_{0.2}O_{3-\delta}$ powder The precursor's $Ba(NO_3)_2$, $Zr(NO_3)_2$, $Ce(NO_3)_3$, and $Y(NO_3)_3$ in the stoichiometric ratio were dissolved in a mixture of water, citric acid, and glycine used as chelating agents in the molar ratio of 1:2:1. The solution was heated at 100 °C and was constantly stirred till it becomes colorless. The solution was frozen in liquid nitrogen and then dehydrated in a vacuum freeze dryer for 48 h. The dried precursor was then heated at 350 °C for 2 h to remove the organic residues through combustion. Afterward, it was calcined at a temperature of 1100 °C for 10 h and finally, a white powder of $BaCe_{0.7}Zr_{0.1}Y_{0.2}O_{3-\delta}$ was obtained.

Sintering aids addition

Sintering aid precursors such as $Bi(NO_3)_3$ and $Cu(NO_3)_2$ each in mole% of 0, 1, 2, and 3 were added to $BaCe_{0.7}Zr_{0.1}Y_{0.2}O_{3-\delta}$ via solvent evaporation method. Firstly, $Bi(NO_3)_3$, $Cu(NO_3)_2$ were dissolved and constantly stirred in acetone and water respectively at constant stirring. Solutions were then mixed and added to $BaCe_{0.7}Zr_{0.1}Y_{0.2}O_{3-\delta}$ powder. The mixed solution was further heated under constant stirring until all the solvent was evaporated and powder was left at the bottom. The dried powder was calcined at a temperature of 800 °C. The calcined powder was grounded by using mortar and pestle. For convenience, the as-prepared powders were labeled as BCZY, BCZY-1, BCZY-2, and BCZY-3 for 0, 1, 2, and 3 mol% of sintering aids respectively. The powders were pellet pressed into 15 mm of diameter under the pressure of 280 MPa and the pellets were sintered in a furnace according to the sintering curve shown in Fig. 1(a and b).

Characterization

X-ray diffractometer (XRD, RigakuD/Max-2400) with Cu-Kα radiation operated at 30 mA and 40 kV was utilized for phase analysis. Microstructure and morphology was examined through Field emission scanning electron microscopy (FESEM, MIRA3 TESCAN). The distribution of sintering aids within sintered pellets was analyzed by Energy Dispersive Spectroscopy (EDS, Oxford Instruments). Four-probe DC-meter (Keithley 2400) measured resistance for the sintered pellets at various temperatures ranging from (450–750) °C in the H_2 atmosphere. Thermochemical changes were investigated through Thermal gravitational analysis and differential scanning calorimetry (TGA/DSC, PerkinElmer).

Linear shrinkage (%) in diameter for sintered pellets was determined by Equation (1);

$$shrinkage\% = \frac{\Delta L}{L} \times 100 \quad (1)$$

Scherer Equation (2) calculated the crystallite size for sintered pellets;

$$D = \frac{K\lambda}{\beta \cos\theta} \quad (2)$$

whereas.

D = crystallite size; K=Scherrer constant; λ = X-ray wavelength CuK_α; β = Line broadening at FWHM; and θ = Bragg's diffraction angle;

Conductivity for the pellets was calculated with the help of Equation (3);

$$\sigma = \frac{D}{RS} \quad (3)$$

whereas.

σ = Conductivity; D = Thickness of sample; R = Resistance; and S= Surface area;

The activation energy was calculated through the Arrhenius plot by using Equation (4);

$$\sigma = \frac{A}{T}\exp\left(\frac{E_a}{K_B T}\right) \quad (4)$$

whereas.

σ = Conductivity; T = Absolute temperature; A = Pre exponential factor; K_B= Boltzmann constant; and E_a = Activation energy.

Results

Thermal analysis of prepared powder

The as-prepared powders were thermally analyzed through TGA/DSC in presence of air atmosphere at a temperature ranging from 30 to 1000 °C (with 5 °C/min heating rate TGA/DTG curves revealed weight loss of −1.8% and −2.2% at a temperature range of (200–300) °C and (700–800) °C. DSC curve showed multiple exothermic peaks attributing towards the removal of NO_x and O_2 due to decomposition of $Cu(NO_3)_2$ and $Bi(NO_3)_3$ respectively. The decomposition reactions for $Cu(NO_3)_2$ and $Bi(NO_3)_3$ are as follow:

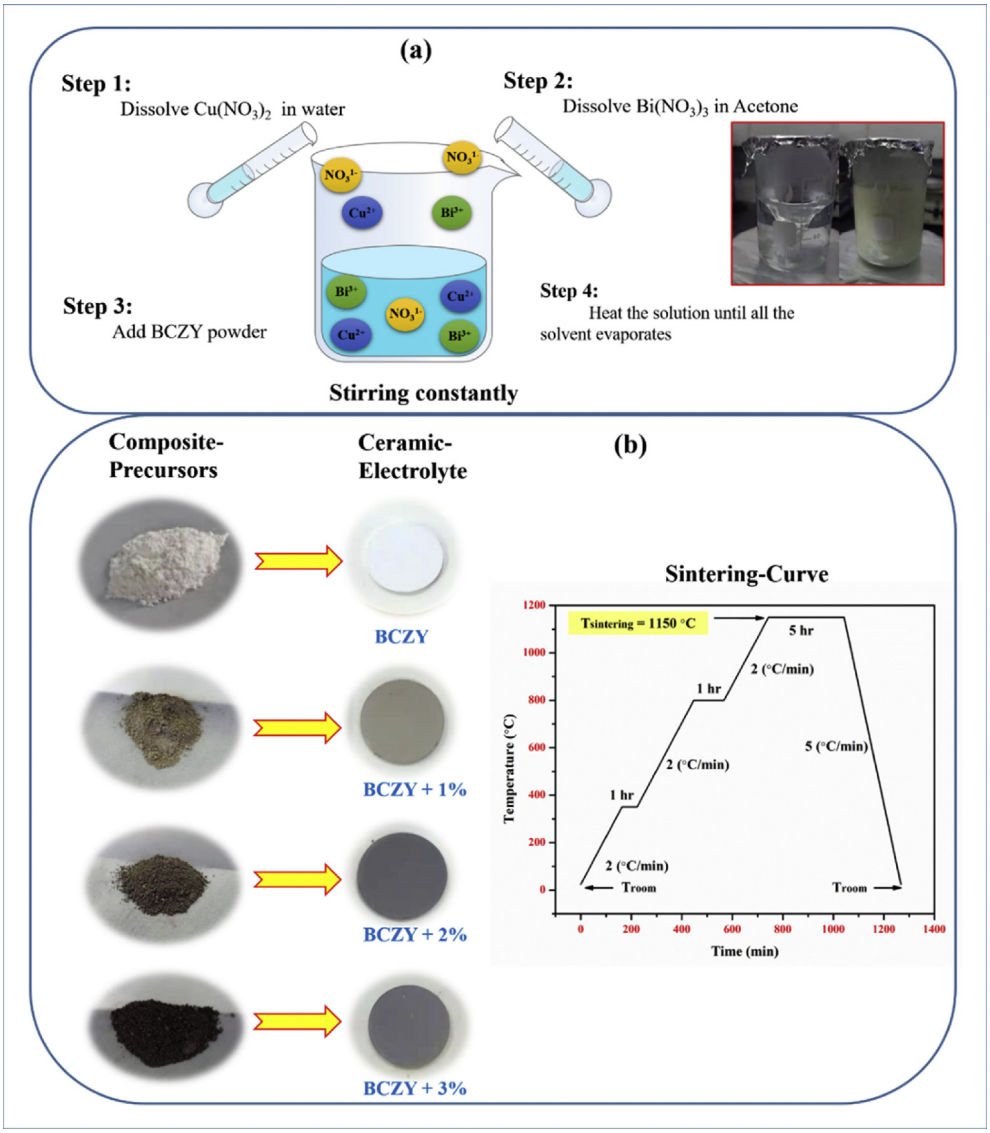

Fig. 1 – (a) Schematic details of sintering aids addition to BCZY via solvent evaporation method (b) Sintering curve.

$$2Cu(NO_3)_2 \xrightarrow{\Delta} 2CuO + 4NO_2 + O_2 \quad (5)$$

$$4Bi(NO_3)_3 \xrightarrow{\Delta} 2Bi_2O_3 + 12NO_3 + 3O_2 \quad (6)$$

An endothermic peak in the DSC curve at a temperature of 824 °C was due to the melting of the Bi_2O_3 phase responsible for the rearrangement of the particles at low temperature, necessary for the dense structure during the sintering process as shown in Fig. 2.

Phase analysis

The XRD patterns for BCZY, BCZY-1, BCZY-2, and BCZY-3 are depicted in Fig. 3. The patterns revealed the complete perovskite phase formation without any impurities for all the synthesized samples sintered at 1150 °C. The perovskite structure remained stable without any secondary phases even after the addition of sintering additives. This may be due to the reason that the amount of sintering additives was very low and was not detected by XRD. With the addition of sintering additives, the peak was shifted towards the lower angle indicating the expansion of crystal lattice. The peak shift was due to the incorporation of Cu^{2+} at B-site Cu^{2+} preferably occupied B-site as compared to Bi^{3+} due to the fact that its ionic radius is closer to Ce^{4+}. Oxygen vacancies were generated due to the replacement of Ce^{4+} with Cu^{2+} attributing towards the loosening of ionic bond which leads to lattice expansion, proposed by Tao and Irvine [43]. The defect reaction for the formation of oxygen vacancies at the A-site is expressed as below;

$$CuO \xrightarrow{BaCeO_3} Cu''_{Ce} + V''_{Ba} + 2V^{\cdot\cdot}_{o} + O_o \quad (7)$$

The crystallite size was reported as increased with the increasing amount of sintering aids. Table 1 describes that crystallite size was increased from (34.3–56.1) nm with the addition of 3 mol% of sintering aid.

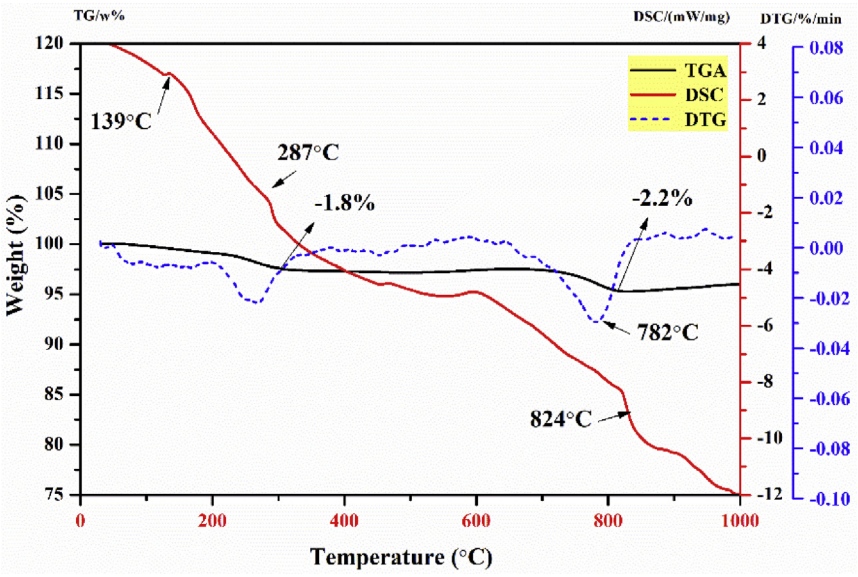

Fig. 2 – TGA/DSC curve for BCZY-2.

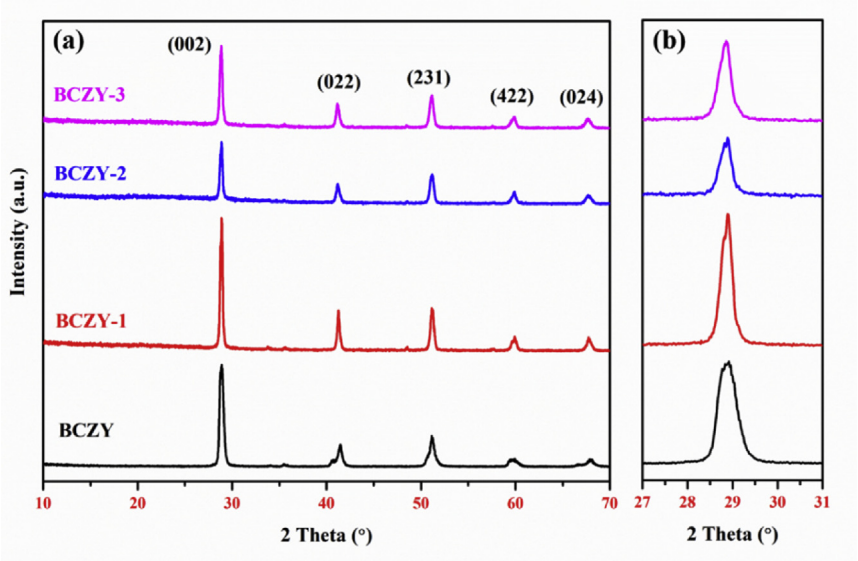

Fig. 3 – (a) XRD patterns for BCZY pellets sintered at 1150 °C with 0, 1, 2, and 3 mol% sintering aids (b) enlarged XRD pattern of (002) diffraction peak.

Table 1 – Crystallite and grain size of BCZY-based electrolyte sintered at 1150 °C for 5 h.

Samples	FWHM	Crystallite size (nm)	Grain size (μm)
BCZY	0.474	34.3	0.35
BCZY-1	0.344	48.7	0.74
BCZY-2	0.324	52.1	1.05
BCZY-3	0.303	56.1	1.3

Sintering behavior and microstructural analysis

Microstructural studies for the prepared powders were carried out by FESEM. Non-uniform particle size distribution with agglomeration was depicted for all the prepared samples as displayed in Fig. 4(a–d).

FESEM images for the surface of the pellets sintered at 1150 °C are shown in Fig. 5(a–d). The additives made it possible to sinter BCZY at a temperature as low as 1150 °C. Sintering additives have decreased the sintering temperature as well as improved the densification with almost no porosity. The grain size was also increased with the increased amount of sintering additives. Liquid phase formation of Bi_2O_3 due to its low melting point promoted the rearrangement of particles at grain boundaries. Lattice distortion and hence increased mobility of grain boundaries during the sintering process was occurred due to the smaller ionic size of Cu^{2+} as compared to Ce^{4+}. The grain growth was also influenced due to the replacement of Ce^{4+} with Cu^{2+} at B-site attributing towards the oxygen vacancies due to charge imbalance condition. Linear shrinkage of pellets was occurred with increased

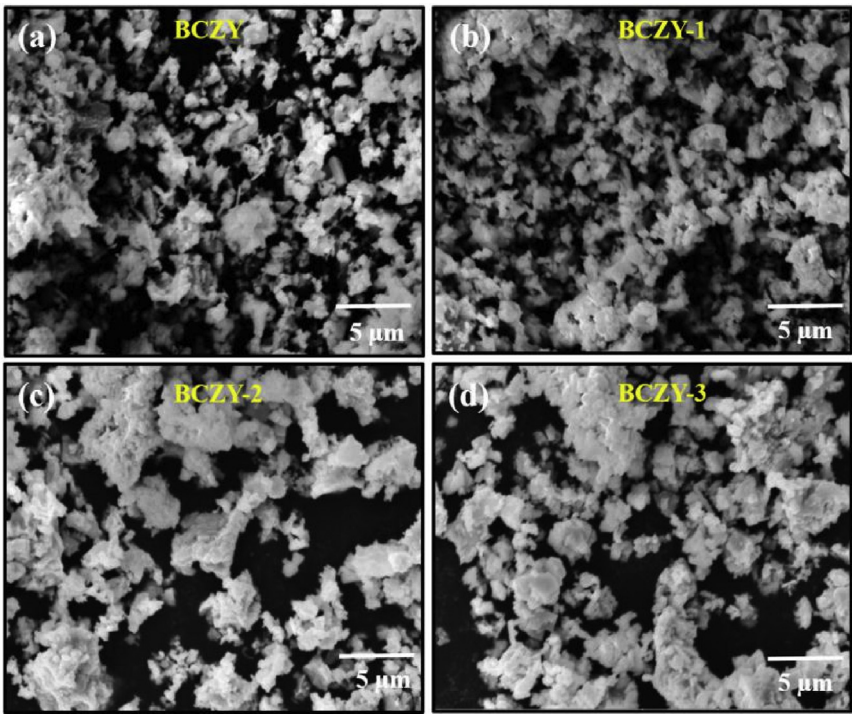

Fig. 4 – FESEM images for (a) BCZY (0 mol %), (b) BCZY-1 (1 mol %), (c) BCZY-2 (2 mol %) and (d) BCZY-3 (3 mol %).

addition of sintering aids as shown in Fig. 5(e). Linear shrinkage of 5% was measured for BCZY whereas, the samples BCZY-1, BCZY-2, and BCZY-3 were reported with linear shrinkage of 18.1, 19.5, and 21% respectively. The required sintering temperature for BCZY is usually above 1500 °C. However, it got a porous and fragile structure when it is sintered at low temperatures such as 1150 °C due to of lack of grain growth and grain boundaries mobility.

Fig. 6(a–d) depicts cross-sectional FESEM images for the fractured pellets. It was observed that sintering additives have reduced the sintering temperature along with internal porosity. BCZY-1 has shown a little porosity at the close-end however, BCZY-2 and BCZY-3 were observed with no porosity at all. EDS mapping for BCZY-1, BCZY-2, and BCZY-3 pellets sintered at 1150 °C are displayed in Fig. 6(e–g). Sintering additives were uniformly distributed with no agglomeration contributing effectively to the densification of the structure. However, in sample BCZY-3, a secondary phase of Y_2O_3 was detected due to a higher concentration of sintering aids hence, more B-sites were created for Cu^{2+}.

EIS measurement

Impedance curves for BCZY-2 and BCZY-3 in dry hydrogen at different temperatures are shown in Fig. 7(a and b). Semicircle at higher frequency was due to bulk response, grain boundary polarization is represented with the second semicircle, whereas, the third semicircle is related with electrode performance. Furthermore, at elevated temperatures, the arcs related to bulk and grain boundary were merged together. The higher frequency intercept at x-axis provided the values of resistance for BCZY-2 and BCZY-3 which are 8 Ωcm^2, 9.4 Ωcm^2 (at 750 °C) and 10.5 Ωcm^2, 12 Ωcm^2 (at 600 °C) respectively. To extract more precise values of resistance, an equivalent circuit was made to fit the obtained data. The fitted lines in the graph along with the circuit are shown inset of Fig. 7(a and b). The conductivities measured for BCZY-2, BCZY-3 at a temperature of 750 °C were 1.07×10^{-2} Scm^{-1} and 0.95×10^{-2} Scm^{-1} respectively as presented in Fig. 7(c).

Relatively higher conductivity was obtained for the sample with additive content as 2 mol% in comparison to that of 3 mol %. The difference in conductivities was indicated prominently at a lower temperature. The low content of additives have promoted the densification and sintering process for BCZY ceramics whereas, higher content had negative effects upon the conductivity. The increased amount of sintering additives initiated the accumulation of secondary phases at the ends of grain boundaries attributing towards the increased resistance. Activation energies were significantly varied with varying temperatures as displayed by the Arrhenius plot in Fig. 7(d). Activation energies ~0.2 eV, 0.28 eV at (1023-823 K) and 0.41 eV, 0.51 eV at (823-723 K) were recorded for BCZY-2 and BCZY-3 respectively.

Discussion

Elevated sintering temperature in preparation of BCZY hinders its utilization in fuel cell applications. Evaporation of barium and segregation of dopants at higher temperatures can greatly affect the conductivity and stability of BCZY as an electrolyte. Moreover, during cell preparation electrolyte prepared at higher sintering temperature causes porosity resulting in the decrease of triple-phase conducting boundaries and

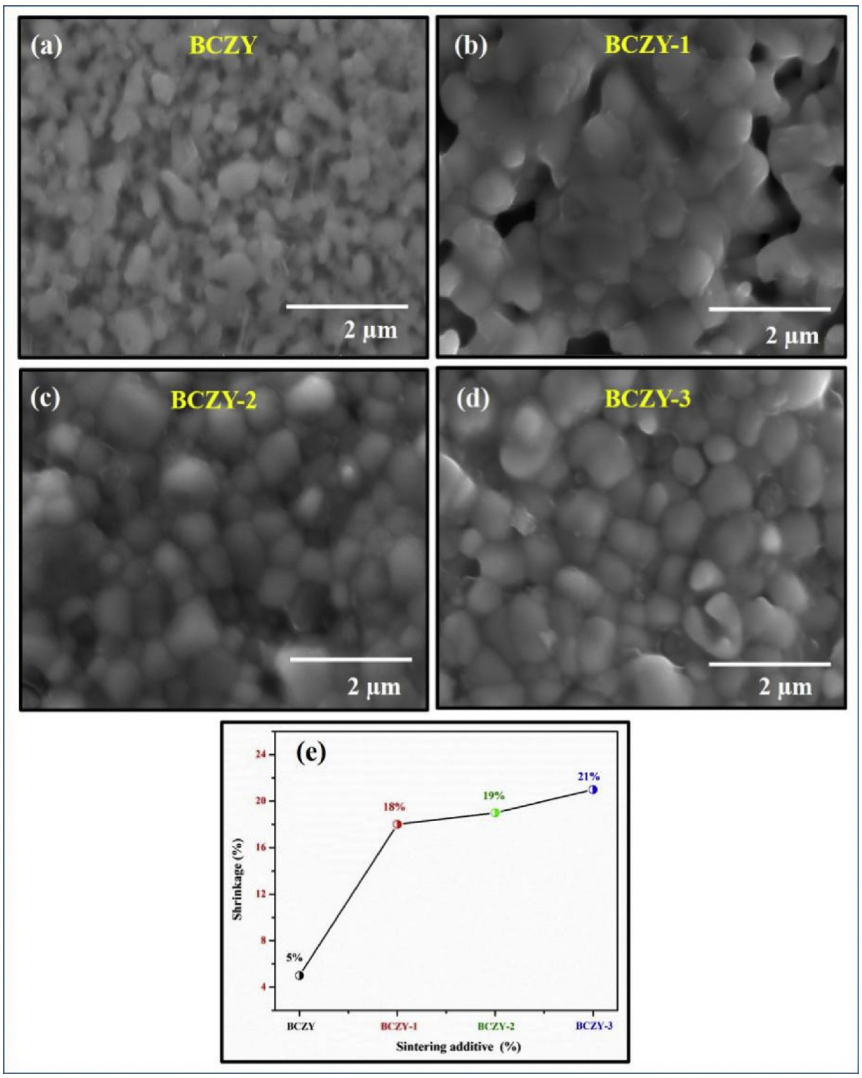

Fig. 5 – FESEM images for surface of (a) BCZY, (b) BCZY-1, (c) BCZY-2, (d) BCZY-3, (e) shrinkage plot for pellets sintered at 1150 °C for 5 h.

hence the performance of the cell. Sintering of BCZY at low temperature is responsible for poor sinterability and greater porosity, highly undesirable for electrolytes because, it can cause gas leakage and low cell performance.

To improve the sinterability at low temperatures without deteriorating its other characteristics a combination of Bi_2O_3 and CuO was introduced into BCZY electrolyte. Bi_2O_3 exhibiting low melting temperature was proved very supportive in particle rearrangement. The endothermic curve in the DSC plot (Fig. 2) at a temperature of 824 °C is attributed towards the melting of Bi_2O_3 and the formation of the liquid phase played a crucial role in the formation of multisite during the sintering process. EDX elemental mapping (Fig. 6) for the sintered pellets (Fig. 6) revealed a homogeneous distribution of Bi_2O_3 and CuO throughout the electrolyte. Homogeneous distribution and non-agglomeration prevented the porosity and cracks within the sintered electrolyte. The liquid phase of Bi_2O_3 was considered as the first driving force towards the sinterability of BCZY electrolyte contributing to the movement of the particles at low temperatures. However, it was not helpful in grain growth to prevent the electrolytic porosity. Grain growth and fusion of grains together are crucial to prevent the porosity and hence densification of the samples is improved. CuO had a significant role in grain growth due to the incorporation of Cu^{2+} in the crystal structure of BCZY attributing towards the dense structure at low temperature ~1150 °C.

The ionic radii for Cu^{2+} and O^{2-} at six-coordination are 0.073 nm, 0.140 nm are resulting in $rCu^{2+}/rO^{2-} = 0.52$. According to Pauling's rules, Cu^{2+} filled the interstice of the octahedron formed by O^{2-} and a stable configuration was obtained. Since the ionic radius of Cu^{2+} (0.073 nm) is closer to Ce^{4+} (0.097 nm) as compared to Ba^{2+} (0.135 nm) therefore, it preferably replaced Ce^{4+} at B-site instead of Ba^{2+} at A-site within ABO_3 perovskite structure. XRD plot (Fig. 3) indicated the shift in diffraction peaks towards the lower angle due to lattice expansion. Oxygen vacancies were generated to compensate for the charge due to the smaller size of Cu^2 than Ce^{4+}. Weak ionic bonding was exhibited due to the formation of more oxygen vacancies contributing towards lattice expansion. Grain-boundary mobility and grain growth were

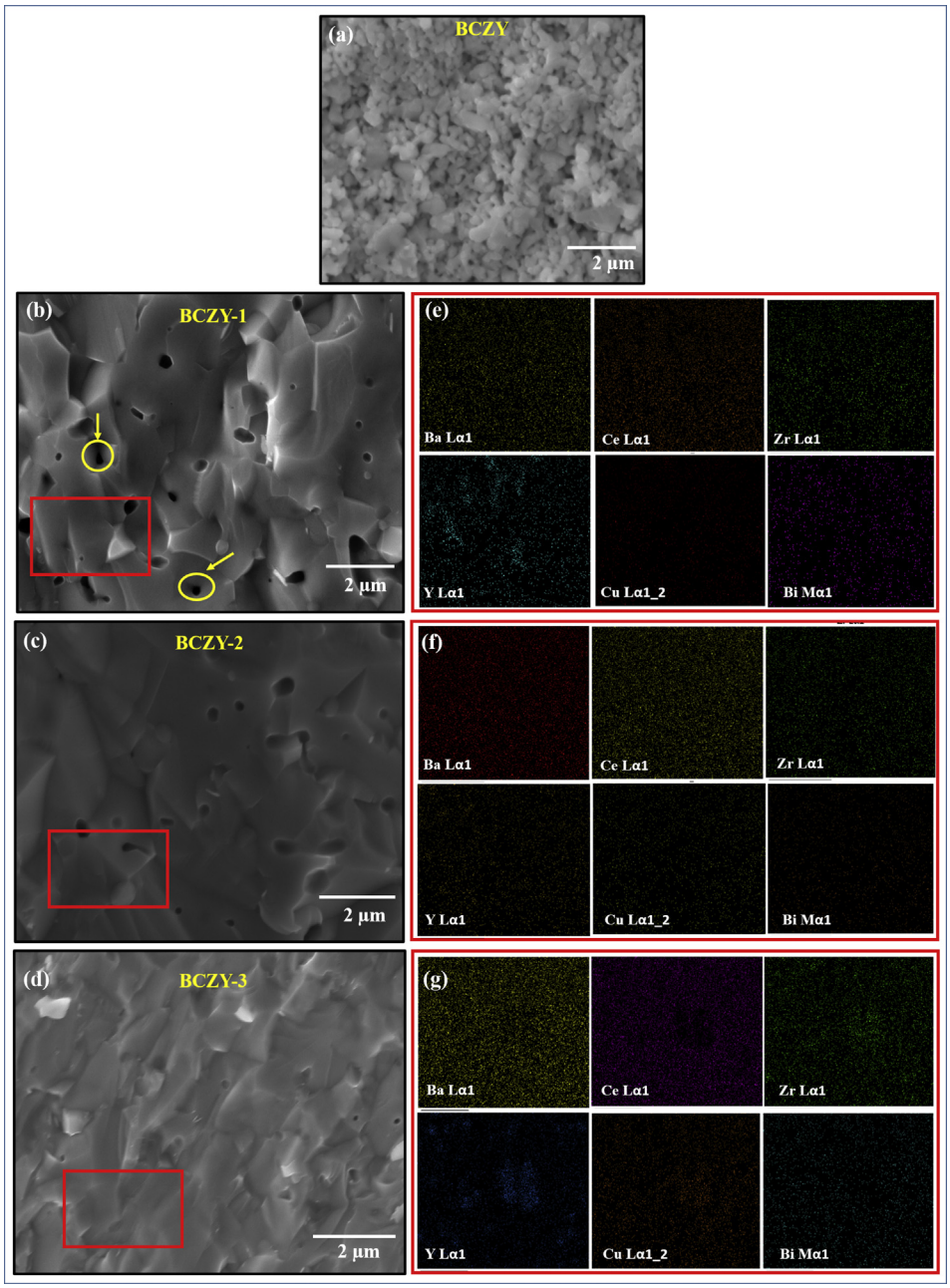

Fig. 6 – Cross sectional FESEM images for fractured pellets (a) BCZY, (b) BCZY-1. (c) BCZY-2, (d) BCZY-3 and the EDS spectrum for BCZY-1 (e), BCZY-2 (f), BCZY-3 (g) respectively.

increased due to the diffusion of Cu^{2+} into crystal structure. Furthermore, the grains were fused together, hence porosity was decreased and density was increased. Grain growth was lacked and porous structure was developed by the samples without sintering aid as shown in Fig. 6.

Conductivities for BCZY-2 and BCZY-3 electrolyte sintered at 1150 °C in the temperature range of (450–750) °C measured in dry H_2 is depicted in Fig. 7(c). Oxygen ion deficient perovskite structure exhibiting A-site formation was obtained with the addition of 2 mol% of sintering aids. Perovskite material was modified to proton conducting material due to hole generation when lower valence element such as Cu^{2+} was accommodated at tetravalent B-site. The following mechanism is followed for conduction in the hydrogen atmosphere [13,14,47,48].

$$H_2 + 2h^{\cdot} + 2O_o^{\times} \leftrightarrow 2(OH)_o^{\cdot} \quad (8)$$

Thus, the conductivity was increased due to enhanced density and additional proton defects. Density was further improved with the increase in sintering aids up to 3 mol% however a slight decrease in conductivity was obtained due to, various defects, lattice distortion, and second phase formation of Y_2O_3 as explained in EDS mapping (Fig. 6). A similar study was carried out about the conductivity of A-site deficient $BaCeO_3$ [49,52,53]. Furthermore, the activation energy for BCZY-3 was enhanced up to 0.51 eV as compared to BCZY-2

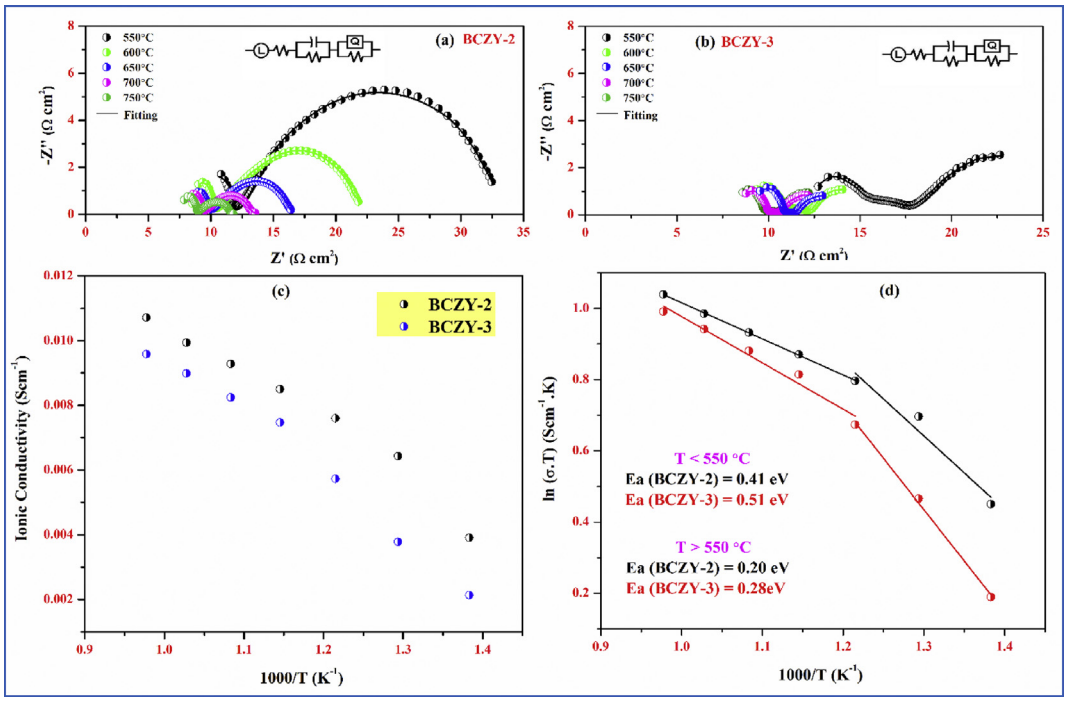

Fig. 7 – EIS (a–b), Conductivity plot (c), Arrhenius plot for (d) BCZY-2 and BCZY-3 at different temperatures.

with activation energy ~0.41 eV as mentioned in the Arrhenius plot (Fig. 7(d)).

Table 2 compares the previously used sintering additives and their conductivities to the present work. 10 wt% ZnO doped into BCZY decreased the sintering temperature up to 1325 °C with conductivity measurement of 1.0×10^{-2} Scm^{-1} (at 600 °C in wet 5% H_2) [46]. The lowest sintering temperature ~1100 °C for BCZY based proton conducting electrolyte was reported when 2 wt% ZnO was added to BCZY, whereas the sintering aids such as NiO, FeO, and CuO could only reduce it up to 1400 °C. However, the conductivity of BCZY sintered at 1100 °C doped with ZnO as sintering aid was lesser than other sintering additives. BCZY with 2 wt% ZnO exhibited a conductivity value ~0.42×10^{-2} Scm^{-1} in wet H_2 [44] while the conductivity for BCZY with 2 mol% $Ni_{0.5}Fe_{0.5}$ was ~0.5×10^{-2} Scm^{-1} in air atmosphere [37]. In the present case BCZY-2, with 2 mol% of CuO and Bi_2O_3 decreased the sintering temperature up to 1150 °C whereas the conductivity calculated at 600 °C in dry H_2 was much more than previously reported sintering aids. The highest conductivity and lowest activation energy for the BZCY-2 sample categorized it as a promising electrolytic candidate for SOFCs operated at intermediate temperatures. Fig. 8 shows the schematic illustration of BCZY with and without CuO-Bi_2O_3 as sintering aids.

To conclude this research work, BZCY was successfully sintered at low temperatures with the help of CuO-Bi_2O_3 as sintering additives. The low activation energy ~0.41 eV at the intermediate temperature indicated the oxygen vaccines attributed towards the ionic conduction throughout the

Table 2 – Sintering temperature and conductivities of BCZY based proton-conducting electrolytes with sintering additives.

Composition	Sintering Temperature (°C)	Measurement Temperature (°C)	Atmospheric Conditions	Conductivity σ(Scm^{-1})	Ref
$BaCe_{0.7}Zr_{0.1}Y_{0.2}O_{3-\delta}$ + 2 mol % $Ni_{0.5}Fe_{0.5}$	1400	700	Air	0.5×10^{-2}	[37]
$BaCe_{0.5}Zr_{0.3}Y_{0.2}O_{3-\delta}$ + 4 mol% ZnO + 0.5 mol% Na_2CO_3	1320	700	3% H_2O-H_2	0.77×10^{-2}	[38]
$BaCe_{0.35}Zr_{0.5}Y_{0.15}O_{3-\delta}$ + 2 wt% ZnO	1100	700	Wet H_2	0.402×10^{-2}	[44]
$BaCe_{0.3}Zr_{0.55}Y_{0.15}O_{3-\delta}$ + 1 wt% NiO	1400	500	Wet H_2	0.117×10^{-2}	[45]
$BaCe_{0.3}Zr_{0.55}Y_{0.15}O_{3-\delta}$ + 1 wt% CuO				0.148×10^{-2}	
$BaCe_{0.3}Zr_{0.55}Y_{0.15}O_{3-\delta}$ + 1 wt% ZnO				0.1124×10^{-2}	
$BaCe_{0.7}Zr_{0.1}Y_{0.1}Zn_{0.1}O_{3-\delta}$ + 10 wt% ZnO	1200	600	Wet 5% H_2	0.859×10^{-2}	[46]
			Dry H_2	0.667×10^{-2}	
$BaCe_{0.5}Zr_{0.3}Y_{0.16}Zn_{0.04}O_{3-\delta}$	1325	600	wet 5% H_2	1×10^{-2}	[29]
$BaZr_{0.1}Ce_{0.66}Ni_{0.04}Y_{0.2}O_{3-\delta}$	1400	600	Wet H_2	0.63×10^{-2}	[27]
$BaCe_{0.7}Zr_{0.1}Y_{0.2}O_{3-\delta}$-2%CuO-$Bi_2O_3$ (BCZY-2)	1150	600	Dry H_2	0.85×10^{-2}	This work
$BaCe_{0.7}Zr_{0.1}Y_{0.2}O_{3-\delta}$-2%CuO-$Bi_2O_3$ (BCZY-3)				0.74×10^{-2}	

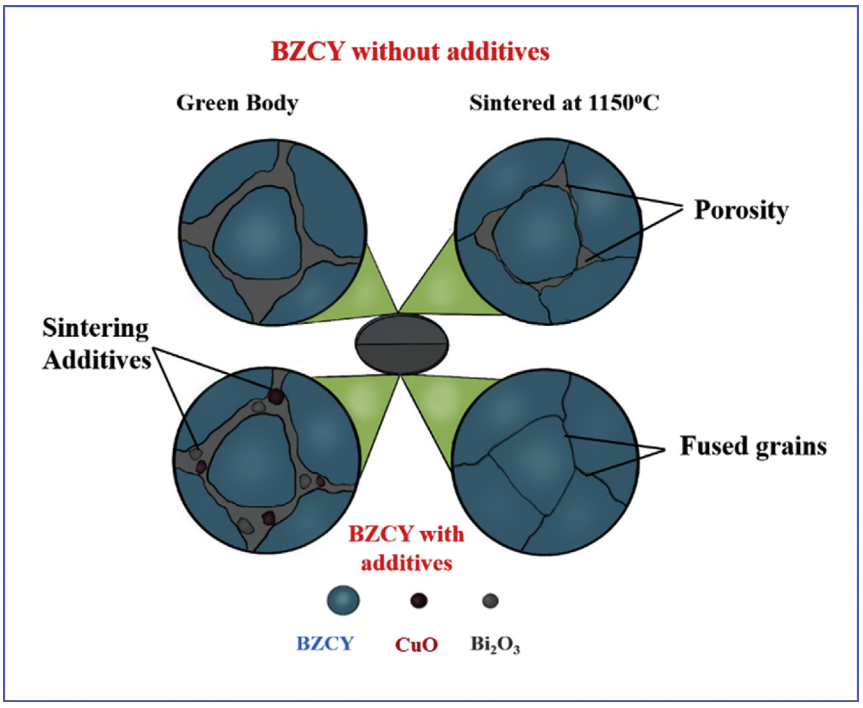

Fig. 8 – Schematic illustration of BCZY with and without CuO-Bi_2O_3 as sintering aids.

electrolyte. The sample with sintering aids of 2 mol % was developed into a dense structure exhibiting minimal activation energy. A structure of perfect density with minimum porosity was also obtained when the percentage of sintering aid was increased from 2 mol % to 3 mol% however, the activation energy and ohmic resistance of electrolyte were increased significantly. Ionic conduction was hindered due to secondary phases with the increased amount of sintering aids. This approach of lowering the sintering temperature of BCZY was found effective to fabricate SOFC s with better performance at a larger scale.

Conclusion

A combination of sintering aids i.e., CuO-Bi_2O_3 in 2–3 mol% was found effective to sinter BCZY at temperatures as low as 1150 °C.

- ✓ $BaCe_{0.7}Zr_{0.1}Y_{0.2}O_{3-\delta}$-2%CuO-$Bi_2O_3$ (BCZY-2) pellets sintered at 1150 °C exhibited a linear shrinkage ~19% with no surface and internal porosity.
- ✓ Crystallite size and grain growth both were improved with the addition of sintering aids. Crystallite size for BCZY was increased from 34.3 nm up to 52.1 nm with 2 mol% of sintering aids.
- ✓ BCZY-2 exhibited a conductivity ~0.85 × 10^{-2} Scm^{-1} at a temperature of 600 °C, which was reduced with the addition of 3 mol% sintering aids.
- ✓ Activation energy for BCZY-2 was calculated ~0.2 eV (at 1023–823 K) and 0.41 eV (at 823–723 K) attributing towards the excellent proton conduction at intermediate temperature.

Declaration of competing interest

The authors declare that they have no known competing financial interests or personal relationships that could have appeared to influence the work reported in this paper.

Acknowledgment

This work was supported by the National Key Research and Development Program of China (Basic Research Project, Grant No. 2017YFB0306100) and the National Key Research and Development Program of China (China-USA Intergovernmental Cooperation Project, Grant NO. 2017YFE0105900) and supported by 111 Project 2.0 (BP0618008).

REFERENCES

[1] Shaheen K, Suo H, Shah Z, Hanif MB, Hussain Z, Ali S, Wang Y. Electrochemical performance of multifuel based nanocomposite for solid oxide fuel cell. Ceram Int 2020;46:8832–8.

[2] Hanif MB, Gao JT, Shaheen K, Wang YP, Yasir M, Li CJ, Li CX. Highly active and novel A-site deficient symmetric electrode material $(Sr_{0.3}La_{0.7})_{1-x}(Fe_{0.7}Ti_{0.3})_{0.9}Ni_{0.1}O_{3-\delta}$ and its effect on electrochemical performance of SOFCs. Int J Hydrogen Energy 2021;46:8778–91.

[3] Hanif MB, Gao JT, Shaheen K, Wang YP, Yasir M, Zhang SL, Li CX. Performance evaluation of highly active and novel $La_{0.7}Sr_{0.3}Ti_{0.1}Fe_{0.6}Ni_{0.3}O_{3-\delta}$ material both as cathode and anode for intermediate-temperature symmetrical solid oxide fuel cell. J Power Sources 2020;472:228498.

[4] Shaheen K, Shah Z, Gulab H, Hanif MB, Faisal S, Suo H. Metal oxide nanocomposites as anode and cathode for low temperature solid oxide fuel cell. Solid State Sci 2020;102:106162.

[5] Hanif MB, Gao JT, Shaheen K, Wang YP, Yasir M, Li CJ, Li CX. Microstructural analysis of highly active cathode material $La_{0.7}Sr_{0.3}Ti_{0.15}Fe_{0.65}Ni_{0.2}O_{3-\delta}$ (LSTFN) by optimizing different processing parameters. Ceram Int 2021;47:10893–904.

[6] Yang H, Hanif MB, Zhang SL, Li CJ, Li CX. Sintering behavior and electrochemical performance of A-site deficient $Sr_xTi_{0.3}Fe_{0.7}O_{3-\delta}$ oxygen electrodes for solid oxide electrochemical cells. Ceram Int 2021;47(17):25051–8.

[7] Zuo C, Zha S, Liu M, Hatano M, Uchiyama M. Ba $(Zr_{0.1}Ce_{0.7}Y_{0.2})O_{3-\delta}$ as an electrolyte for low-temperature solid-oxide fuel cells. Adv Mater 2006;18:3318–20.

[8] Heras-Juaristi G, Pérez-Coll D, Mather GC. Temperature dependence of partial conductivities of the $BaZr_{0.7}Ce_{0.2}Y_{0.1}O_{3-\delta}$ proton conductor. J Power Sources 2017;364:52–60.

[9] Yang L, Wang S, Blinn K, Liu M, Liu Z, Cheng Z, Liu M. Enhanced sulfur and coking tolerance of a mixed ion conductor for SOFCs: $BaZr_{0.1}Ce_{0.7}Y_{0.2-x}Yb_xO_{3-\delta}$. Science 2009;326:126–9.

[10] Guo Y, Lin Y, Ran R, Shao Z. Zirconium doping effect on the performance of proton-conducting $BaZryCe_{0.8-y}Y_{0.2}O_{3-\delta}$ ($0.0\leq y\leq 0.8$) for fuel cell applications. J Power Sources 2009;193:400–7.

[11] Babilo P, Uda T, Haile SM. Processing of yttrium-doped barium zirconate for high proton conductivity. J Mater Res 2007;22:1322–30.

[12] Münch W, Kreuer KD, Seifert G, Maier J. Proton diffusion in perovskites: comparison between $BaCeO_3$, $BaZrO_3$, $SrTiO_3$, and $CaTiO_3$ using quantum molecular dynamics. Solid State Ionics 2000;136:183–9.

[13] Kreuer KD, Münch W, Fuchs A, Klock U, Maier J. Proton conducting alkaline earth zirconates and titanates for high drain electrochemical applications. Solid State Ionics 2001;145:295–306.

[14] Kreuer KD. Proton-conducting oxides. Annu Rev Mater Res 2003;33:333–59.

[15] Peng C, Melnik J, Luo JL, Sanger AR, Chuang KT. $BaZr_{0.8}Y_{0.2}O_{3-\delta}$ electrolyte with and without ZnO sintering aid: preparation and characterization. Solid State Ionics 2010;181:1372–7.

[16] Gui L, Ling Y, Li G, Wang Z, Wan Y, Wang R, Zhao L. Enhanced sinterability and conductivity of $BaZr_{0.3}Ce_{0.5}Y_{0.2}O_{3-\delta}$ by addition of bismuth oxide for proton conducting solid oxide fuel cells. J Power Sources 2016;301:369–75.

[17] Chen L, Wang Y, Zhu XF, Meng J. Enhanced sintering of $Ce_{0.8}Nd_{0.2}O_{2-\delta}$-$La_{0.8}Sr_{0.2}Ga_{0.8}Mg_{0.2}O_{3-\delta}$ using CoO as a sintering aid. Ceram Int 2017;43:3583–9.

[18] Wang B, Bi L, Zhao XS. Exploring the role of NiO as a sintering aid in $BaZr_{0.1}Ce_{0.7}Y_{0.2}O_{3-\delta}$ electrolyte for proton-conducting solid oxide fuel cells. J Power Sources 2018;399:207–14.

[19] Lee KR, Tseng CJ, Jang SC, Lin JC, Wang KW, Chang JK, Lee SW. Fabrication of anode-supported thin BCZY electrolyte protonic fuel cells using NiO sintering aid. Int J Hydrogen Energy 2019;44:23784–92.

[20] Sun Z, Fabbri E, Bi L, Traversa E. Lowering grain boundary resistance of $BaZr_{0.8}Y_{0.2}O_{3-\delta}$ with $LiNO_3$ sintering-aid improves proton conductivity for fuel cell operation. Phys Chem Chem Phys 2011;13:7692–700.

[21] Long Y, Huang L, Che J, Lin HT, Zhang F. Role of MgO on densification and mechanical properties in spark plasma sintered $Os_{0.9}Re_{0.1}B_2$ ceramic. Ceram Int 2020;46:2612–7.

[22] Gao D, Guo R. Structural and electrochemical properties of yttrium-doped barium zirconate by addition of CuO. J Alloys Compd 2010;493:288–93.

[23] Baral AK, Tsur Y. Sintering aid (ZnO) effect on proton transport in $BaCe_{0.35}Zr_{0.5}Y_{0.15}O_3$-δ and electrode phenomena studied by distribution function of relaxation times. J Am Ceram Soc 2019;102:239–50.

[24] An H, Shin D, Ji HI. Effect of nickel addition on sintering behavior and electrical conductivity of $BaCe_{0.35}Zr_{0.5}Y_{0.15}O_{3-\delta}$. J Kor Chem Soc 2019;56:91–7.

[25] Loureiro FJ, Nasani N, Reddy GS, Munirathnam NR, Fagg DP. A review on sintering technology of proton conducting $BaCeO_3$-$BaZrO_3$ perovskite oxide materials for Protonic Ceramic Fuel Cells. J Power Sources 2019;438:226991.

[26] Liu Z, Wang X, Liu M, Liu J. Enhancing sinterability and electrochemical properties of Ba $(Zr_{0.1}Ce_{0.7}Y_{0.2})O_{3-\delta}$ proton conducting electrolyte for solid oxide fuel cells by addition of NiO. Int J Hydrogen Energy 2018;43:13501–11.

[27] Wang B, Bi L, Zhao XS. Exploring the role of NiO as a sintering aid in $BaZr_{0.1}Ce_{0.7}Y_{0.2}O_{3-\delta}$ electrolyte for proton-conducting solid oxide fuel cells. J Power Sources 2018;399:207–14.

[28] Tong J, Clark D, Bernau L, Subramaniyan A, O'Hayre R. Proton-conducting yttrium-doped barium cerate ceramics synthesized by a cost-effective solid-state reactive sintering method. Solid State Ionics 2010;181:1486–98.

[29] Tao SW, Irvine JT. A stable, easily sintered proton-conducting oxide electrolyte for moderate-temperature fuel cells and electrolyzers. Adv Mater 2006;18:1581–4.

[30] Wang H, Peng R, Wu X, Hu J, Xia C. Sintering behavior and conductivity study of yttrium-doped $BaCeO_3$-$BaZrO_3$ solid solutions using ZnO additives. J Am Ceram Soc 2009;92:2623–9.

[31] Umaru D, Zakaria A, Abdullah CAC, Lakin II, Abdollahi Y. Effect of sintering temperature on V_2O_5 doped ZnO-Bi=O_3-Sb_2O_3-MnO_2 based varistor ceramics: microstructure and electrical properties. Digest J Nanomater Biostruct 2016;11.

[32] Zhang C, Zhao H, Xu N, Li X, Chen N. Influence of ZnO addition on the properties of high temperature proton conductor $Ba_{1.03}Ce_{0.5}Zr_{0.4}Y_{0.1}O_{3-\delta}$ synthesized via citrate–nitrate method. Int J Hydrogen Energy 2009;34:2739–46.

[33] Nikodemski S, Tong J, Duan C, O'Hayre R. Ionic transport modification in proton conducting $BaCe_{0.6}Zr_{0.3}Y_{0.1}O_{3-\delta}$ with transition metal oxide dopants. Solid State Ionics 2016;294:37–42.

[34] Chen X, Sun X, Zhou J, Zhou D, Zhu X, Meng J. Effects of CoO and Bi_2O_3 single/dual sintering aids doping on structure and properties of $Ce_{0.8}Nd_{0.2}O_{1.9}$. Ceram Int 2020;46:22727–32.

[35] Wu C, Yu Z, Wu G, Sun K, Yang Y, Jiang X, Lan Z. Low-temperature sintering of barium hexaferrites with Bi_2O_3/CuO additives. IEEE Trans Magn 2015;51:1–4.

[36] Ma G, We Z, Han J, Zhang J, Wen Y. Enhanced proton conduction of $BaZr_{0.9}Y_{0.1}O_{3-\delta}$ by hybrid doping of ZnO and Na_3PO_4. Solid State Ionics 2015;281:6–11.

[37] Liu Z, Chen M, Zhou M, Cao D, Liu P, Wang W, Liu J. Multiple effects of iron and nickel additives on the properties of proton conducting yttrium-doped barium cerate-zirconate electrolytes for high-performance solid oxide fuel cells. ACS Appl Mater Interfaces 2020;12:50433–45.

[38] YLi Y, Guo R, Wang C, Liu Y, Shao Z, An J, Liu C. Stable and easily sintered $BaCe_{0.5}Zr_{0.3}Y_{0.2}O_{3-\delta}$ electrolytes using ZnO and Na2CO3 additives for protonic oxide fuel cells. Electrochim Acta 2013;95:95–101.

[39] Li Y, Yang W, Wang L, Zhu J, Meng W, He Z, Dai L. Improvement of sinterability of $BaZr_{0.8}Y_{0.2}O_{3-\delta}$ for H2 separation using Li_2O/ZnO dual-sintering aid. Ceram Int 2018;44:15935–43.

[40] Liu L, Zhou Z, Tian H, Li J. Effect of bismuth oxide on the microstructure and electrical conductivity of yttria stabilized zirconia. Sensors 2016;16:369.

[41] Singh P. Influence of Bi_2O_3 additive on the electrical conductivity of calcia stabilized zirconia solid electrolyte. J Eur Ceram Soc 2015;35:1485–93.
[42] Yeh TH, Kusuma GE, Suresh MB, Chou CC. Effect of sintering process on the microstructures of Bi2O3-doped yttria stabilized zirconia. Mater Res Bull 2010;45:318–23.
[43] Tao S, Irvine JT. Conductivity studies of dense yttrium-doped $BaZrO_3$ sintered at 1325 C. J Solid State Chem 2007;180:3493–503.
[44] Baral AK. Reduction in sintering temperature of stable proton conductor $BaCe_{0.35}Zr_{0.5}Y_{0.15}O_{3-\delta}$ prepared by sol–gel method and its transport properties. Solid State Ionics 2015;272:107–11.
[45] Nasani N, Shakel Z, Loureiro FJ, Panigrahi BB, Kale BB, Fagg DP. Exploring the impact of sintering additives on the densification and conductivity of $BaCe_{0.3}Zr_{0.55}Y_{0.15}O_{3-\delta}$ electrolyte for protonic ceramic fuel cells. J Alloys Compd 2021;862:158640.
[46] Hossain S, Abdalla AM, Radenahmad N, Zakaria AKM, Zaini JH, Rahman SH, Azad AK. Highly dense and chemically stable proton conducting electrolyte sintered at 1200 C. Int J Hydrogen Energy 2018;43:894–907.
[47] Hossain S, Abdalla AM, Jamain SNB, Zaini JH, Azad AK. A review on proton conducting electrolytes for clean energy and intermediate temperature-solid oxide fuel cells. Renew Sustain Energy Rev 2017;79:750–64.
[48] Li L, Nino JC. Proton-conducting barium stannates: doping strategies and transport properties. Int J Hydrogen Energy 2013;38:1598–606.
[49] Wu X, Wang H, Peng R, Xia C, Meng G. Effect of A-site deficiency in $BaCe_{0.8}Sm_{0.2}O_{3-\delta}$ on the electrode performance for proton conducting solid oxide fuel cells. Solid State Ionics 2011;192:611–4.
[50] Li Y, Yin B, Fan Y, Huan Y, Dong D, Hu X, Wei T. Achieving high mechanical-strength CH4-based SOFCs by low-temperature sintering (1100 °C). Int J Hydrogen Energy 2020;45:3086–93.
[51] Yang T, Loureiro FJ, Queirós RP, Pukazhselvan D, Antunes I, Saraiva JA. A detailed study of hydrostatic press, sintering aids and temperature on the densification behavior of Ba (Zr, Y) $O_{3-\delta}$ electrolyte. Int J Hydrogen Energy 2016;41:11510–9.
[52] Hanif MB, Motola M, Rauf S, Li CJ, Li CX. Recent advancements, doping strategies and the future perspective of perovskite-based Solid oxide fuel cells for energy conversion. Chem Eng J 2021;428:132603.
[53] Hanif Muhammad Bilal, Rauf Sajid, Motola Martin, Babara Zaheer Ud Din, Li CJ, Li CX. Recent progress of perovskite-based electrolyte materials for solid oxide fuel cells and performance optimizing strategies for energy storage applications. Mater Res Bull 2022;146:111612. https://doi.org/10.1016/j.materresbull.2021.111612.